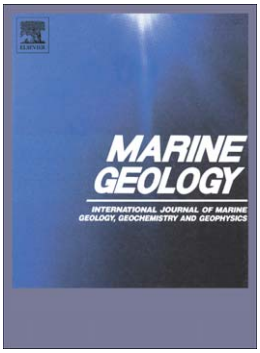

Classification of rocky headlands in California with relevance to littoral cell boundary delineation

D.A. George, J.L. Largier, C.D. Storlazzi, P.L. Barnard

PII: S0025-3227(15)30015-3
DOI: doi: 10.1016/j.margeo.2015.08.010
Reference: MARGO 5328

To appear in: *Marine Geology*

Received date: 25 January 2015
Revised date: 6 August 2015
Accepted date: 8 August 2015

Please cite this article as: George, D.A., Largier, J.L., Storlazzi, C.D., Barnard, P.L., Classification of rocky headlands in California with relevance to littoral cell boundary delineation, *Marine Geology* (2015), doi: 10.1016/j.margeo.2015.08.010

Classification of rocky headlands in California with relevance to littoral cell boundary delineation

DA George[1*], JL Largier[1], CD Storlazzi[2], PL Barnard[2]

Revised submission to *Marine Geology*

1 – Bodega Marine Laboratory, University of California, Davis, P.O. Box 247, Bodega Bay, CA 94923
2 – Pacific Coastal and Marine Science Center, US Geological Survey, 400 Natural Bridges Drive, Santa Cruz, CA 95060
* - corresponding author contact: dgeorge@ucdavis.edu

Abstract

Despite extensive studies of hydrodynamics and sediment flux along beaches, there is little information on the processes, pathways and timing of water and sediment transport around rocky headlands. In this study, headlands along the California coast are classified to advance understanding of headland dynamics and littoral cell boundaries in support of improved coastal management decisions. Geomorphological parameters for 78 headlands were quantified from geological maps, remote-sensing imagery, navigational charts, and shoreline geospatial databases. *K*-means cluster analysis grouped the headlands into eight distinct classes based on headland perimeter, bathymetric slope ratio, and the headland apex angle. Wave data were used to investigate the potential for sediment transport around the headland types and determine the efficacy of the headland as a littoral cell boundary. Four classes of headland appear to function well as littoral cell boundaries, with headland size (e.g., perimeter or area) and a marked change in nearshore bathymetry across the headland being relevant attributes. About half of the traditional California littoral cell boundaries align with headland classes that are expected to perform poorly in blocking alongshore sediment transport, calling into question these boundaries. Better definition of these littoral cell boundaries is important for regional sediment management decisions.

Keywords: headlands; sediment transport; littoral cell boundaries; classification.

1. Introduction

Rocky headlands are prominent morphological features that can deflect or block alongshore currents and sediment transport, focus wave energy, shed eddies, and/or create sediment retention zones (Alaee et al., 2004; Davies et al., 1995; Winant, 2006). Headlands are frequently associated with cliff-backed shorelines, which Emery and Kuhn (1982) observed to comprise approximately 80% of coasts globally. The geological and oceanographic parameters that form and evolve headlands include the balance of wave attenuation vs. refraction, base lithology, the presence of a shore platform, and the strike of the most resistant formation with respect to wave direction (Stuiver, 2013). Presently, many assumptions must be made to characterize relationships between sediment flux, sediment deposits, and morphodynamics around headlands. Despite extensive study offshore of embayed beaches (Loureiro et al., 2012; Sallenger et al., 2002), flow and sediment transport along rocky shores and around headlands remains poorly understood. Some studies have deduced transport from analysis of bed characteristics such as grain size, grain composition, and morphology (Storlazzi and Field, 2000) while geologically-based studies have reported deposition and erosion patterns in the vicinity of headlands in the United Kingdom (Bastos et al., 2002), New Zealand (Hume et al., 2000) and Western Australia (Stul et al., 2012). Other ecological studies have explored the transport of planktonic larvae in the lee of a headland (Roughan et al., 2005). However, mechanistic studies that connect oceanographic processes to sediment transport rates and morphological change are still lacking.

These research gaps and societal needs argue for new research to better understand how headlands affect circulation and transport rates of sediment or biota. A first step is to categorize different types of headlands, based on shape, size, complexity and nearshore bathymetry. Many approaches to grouping environmental phenomena are found in the oceanographic, hydrologic, and geologic disciplines. Examples of classification methods for marine features come from beaches (Scott et al., 2011; Wright and Short, 1984), coral reefs (Freeman et al., 2012), wave climates (Camus et al., 2011), and submarine canyons (Harris and Whiteway, 2011). Developing a classification for headlands would open new avenues for research, both in explaining these headland types (e.g., geological framework or rock types) and in determining the effect of different headland types on flow, sediment transport and associated geomorphology and ecology. The primary aim of this paper is to develop a classification of headlands by identifying key factors that differentiate types of headlands. The secondary goal is to investigate littoral cell boundaries associated with each headland type.

2. Background

Several numerical modeling studies have explored transport around headlands with generic idealized headland designs (Davies et al., 1995; Guillou and Chapalain, 2011; Signell and Geyer, 1991). These studies focused on the hydrodynamics and posited the influence on sediment movement; field measurements were not included. Further, the geometric asymmetry of headlands has also been ignored in numerical modeling studies. Most headlands are not symmetrical, so that two different flow-topography scenarios occur for alongshore flow in two different directions. Denniss et al. (1995)_ENREF_18

identified different spectral energies of currents on either side of Bass Point, Australia, and attributed circulation variability to the complexity of the headland geometry. Asymmetric development of sandbanks on either side of a headland has also been explored through analysis of the Coriolis effect and seabed slope (Jones et al., 2006; Neill and Scourse, 2009).

Extensive research on beach dynamics connects the physical oceanography of water transport (jets, eddies and wakes) to sediment transport. Prior investigations most relevant to this paper focused on headland embayed beaches where the influence of headlands on beach morphology is addressed. The seminal work in this area is by Short (1999), who used observations of Australian beaches to establish a conceptual model of sand bypassing and a non-dimensional embayment scaling parameter. The parameter categorizes beach circulation as 'normal', 'transitional', or 'cellular', with 'cellular' referring to headland-dominated circulation. The relationship informs a conceptual model of sand bypassing by suggesting sediment migrates along a beach toward a headland before conditions are favorable for transport around the apex of the promontory. Loureiro et al. (2012)_ENREF_40 explored the ideas of Short (1999) at six relatively 'small' embayed beaches in Portugal. They suggest that there may be bounds to the upstream length of beaches influenced by headlands. Other headland/embayed beach examples span the globe: Australia (Goodwin et al., 2013), China (Dai et al., 2010), Mexico (Silva et al., 2010), Brazil (de Castilhos and Gre, 2006) and Ireland (Backstrom et al., 2009). More generally, van Rijn (2010) suggests that the most important characteristics of headlands are: 1) convergence points for wave energy; 2) obstruction to alongshore tide-

and wind-induced currents and convergence of currents; 3) large-scale circulation zones downstream of headlands; 4) obstruction to littoral drift; 5) fixation points for seaward rip currents promoting offshore transport; and, 6) fixation points for spit formation and shoals originating from headland erosion.

2.1. Headlands as Littoral Cell Boundaries

In California, 22 of the 25 littoral cells, originally called "coastal compartments" by Inman and Frautschy (1966)_ENREF_31 in southern California and extended statewide by Habel and Armstrong (1978), are either fully or partially defined by headlands, but done so purely qualitatively. Improving knowledge of how headlands affect alongshore transport can impact how society faces two coastal challenges: 1) sediment and pollution management at the local scale, e.g., beach nourishment decisions; and 2) regional scale planning, e.g., marine protected area networks or sediment management. Beach communities throughout the world are facing varying amounts of sea-level rise that threaten coastal infrastructure, tourist- and recreation-based economies, and coastal habitats. Beach nourishment (placement of sand on the shoreline) is used to widen beaches that are naturally narrow or where the natural supply of sand has been significantly reduced through human activities (Patsch and Griggs, 2007). It is a tool that can be used for climate change adaptation as well as sustaining recreational resources. One of the challenges for beach nourishment is estimating the residence time of the sand placed on the beach with many factors influencing sediment transport – wave energy and direction, sediment grain size, alongshore and cross-shore currents. Waves and currents are affected by headlands and the headlands' potential to be a boundary to sediment transport. The second challenge, regional coastal management, connects the littoral cell

concept and its application to conservation efforts. Littoral cells have frequently been set between headlands, although other features such as rivers, inlets, and submarine canyons are also used as boundaries. Successful examples of combining littoral cells with coastal management can be found around the world, including Western Australia (Stul et al., 2012), the United Kingdom (Cooper and Pontee, 2006), and Pacific Ocean island atolls (Collen et al., 2009).

Whereas recognition of littoral cells is an important foundation for coastal planning, it is not clear for which sediment sizes these littoral cells are effective nor how effective. Limber et al. (2008) note the importance of sediment size in accounting for sediment budgets in a littoral cell and Sanderson and Eliot (1999) used cluster analysis of grain sizes to define littoral cells along the west coast of Australia. In reality, some leakage is expected across boundaries, but there is little insight as to when that occurs and thus little ability to project future conditions under climate change scenarios. Davies (1974) questioned the validity of boundaries by suggesting that most boundaries are drawn arbitrarily and noted that littoral cells have varying degrees of connectedness to other cells. van Rijn (2010) proposed three types of alongshore cell boundaries, including both natural and constructed features:

Fixed absolute boundaries – barriers to all sediment (hard rock headlands, long jetties, deep inlets, canyons, navigation channels; long harbor breakwaters);

Fixed partial boundaries – bypassing or periodic (often storm-related) throughput of sediment take place (soft rock/compound cliff type headlands and shallow inlets);

Transient partial boundaries – generally, have a more diffusive character and have limited stability (spits, sand banks, shallow channels, short headlands, short breakwaters).

3. Study Area

The 1,800-km coastline of California is extremely diverse, ranging from steep coastal cliffs, marine terraces, and coastal plains to coastal lagoons and sandy beaches. The coastline is composed of different types of beaches and geological features: approximately 28.4% is pocket beaches, 32.3% is sandy beach, and 39.3% is rocky shoreline (Scholar and Griggs, 1997). Headlands are found in all three coastline types, with particular prominence in creating pocket beaches and defining rocky shorelines. Approximately two-thirds of the coast is oriented north-south from the Oregon border to Point Conception, where it turns east and forms the Southern California Bight as the shoreline curves south to Mexico. The largest interruption to the coast is the entrance to San Francisco Bay, but other large inlets include Humboldt Bay, Tomales Bay, the ports of Los Angeles and Long Beach, and San Diego Bay (Figure 1). Major peninsulas are Monterey Peninsula, Palos Verdes and Point Reyes, while Cape Mendocino, Point Arena and Point Conception represent even larger scale promontories or coastal curvature that exert a first-order effect on shelf-scale circulation (Largier et al., 1993).

The geology of California's headlands is related to the underlying structure and tectonic processes along the coast. Inman and Nordstrom (1971) described the coastline as a transform-fault with attributes of formerly being a collision coast including a narrow shelf, offshore trenches, coastal mountains and hills, and uplifted coastal terraces. The

three geomorphic provinces that comprise the coast (Coast Ranges, Transverse Ranges, and Peninsular Ranges) are primarily continental and marine Mesozoic and Cenozoic sedimentary rock, some of which has been folded and faulted (CGS, 2002, 2006). The vertically and longitudally variable rock type along the coastline helps support the models of headland formation and evolution described by Stuiver (2013) and Limber and Murray (2015). Both include wave activity as a key parameter of headland development, which will be addressed below.

The supply of gravel, sand, and mud that characterize the sediment type offshore of California comes primarily from rivers, with cliff erosion as a secondary source (Milliman and Farnsworth, 2011; Slagel and Griggs, 2008). The largest river systems in either annual water or sediment delivery directly to the Pacific Ocean (as opposed to San Francisco Bay) include the Smith, Klamath, Mad, Eel, Russian, Salinas, Santa Clara, Santa Ana, and Tijuana (Milliman and Farnsworth, 2011). The Sacramento and San Joaquin Rivers, which drain 40% of California, empty into San Francisco Bay. Numerical modeling estimates 1,200,000 t/yr of suspended sediment migrates to the outer coast through the Golden Gate (Erikson et al., 2013). Slagel and Griggs (2008) estimated that approximately 10,000,000 m^3/yr of sand and gravel would be delivered by the 21 major river systems of the state (excluding the Sacramento-San Joaquin) if it were not for the 66 dams that impound 2,300,000 m^3/yr of sediment. Best and Griggs (1991) estimated that statewide, 70-85% of sand delivered to the coast originates from rivers although recent work has suggested otherwise. For example, Perg et al. (2003) found a 50:50 ratio of fluvial vs. terrace contribution in Santa Cruz, whereas Young and Ashford (2006) found

67% of littoral sediment originated from seacliffs in the San Diego area. Comparable values for gravel and fine-grained sediment have yet to be compiled statewide. On the opposite side of littoral transport, submarine canyons are the primary sink for sediment that flows around headlands along California. More than 25 submarine canyons can be identified along the California coast that incise the shelf and extend across the continental slope. The largest and most complex is the Monterey Submarine Canyon in Monterey Bay. Canyons with their heads close to the shoreline are most relevant to alongshore sediment transport. Everts and Eldon (2000) identified five southern California canyons as likely to be actively removing sand from littoral cells by funneling sediment down through the continental rise, such as Mugu, Hueneme, and La Jolla. Building on this work, Covault et al. (2007) found that different canyon-channel systems intercept the littoral cells depending on the shelf width between the canyon head and the littoral zone. On the northern end of the state, Mullenbach et al. (2004) found that the Eel Canyon removed approximately 12% of Eel River sediment delivered to the shelf.

The sediment that reaches the ocean enters a wave-dominated environment. Wingfield and Storlazzi (2007) described the wave climate for central California, but all of California experiences relatively similar patterns with wave energy decreasing from north to south. Three types of wave conditions characterize the nearshore processes over the course of a typical year: northern hemisphere swell, southern hemisphere swell, and local wind-driven seas. The winter months (November-March) are dominated by northern hemisphere swell with maximum significant wave heights that can be larger than 7 m in the northern part of the state but closer to 4 m in the southern section. Summer months

are more quiescent, with southern hemisphere swell on the order of 2-3 m significant wave height and peak wave periods greater than 12 s. Winds and local sea are stronger north of Point Conception, where local wind-driven waves may dominate swell energy.

Currents due to tides and wind forcing are also important for sediment motion along the California coast, particularly the fine grain size classes. The range of the mixed, semi-diurnal tides along the coast increases from south to north, with an average diurnal range of 1.6 m along the open coast in San Diego, up to 2.1 m in Crescent City (NOAA, 2014). With a micro-tidal range, tidal currents are not strong in general, although tidal jets may be observed at the mouth of the larger bays (e.g., San Francisco Bay, Barnard et al. (2012), and San Diego Bay, Chadwick and Largier (1999)). Weaker tidal jets may also occur at headlands, but few observations exist. In central and northern California, subtidal currents outside of the wave-dominated nearshore are primarily wind-driven (e.g., Largier et al. (1993)). Strong northerly winds drive upwelling and a southward shelf jet during much of the year, although exhibiting marked synoptic variability. At times, offshore eddies associated with the California Current may enhance these flows (Kaplan et al., 2009). However, strong shelf currents are slowed by bottom drag in shallow waters near the coast (typically inshore of 30 m) described as a "coastal boundary layer" by Nickols et al. (2012). In winter, strong southerly wind events can lead to fast northward flow with downwelling and significant speeds nearshore (Drake et al., 2005). Typically, the general circulation and wind-driven coastal currents are weaker south of Point Conception in the Southern California Bight.

4. Data Collection and Analysis

Data on geomorphology, including shoreline and bathymetric features, and wave processes were collected, prepared and analyzed as summarized in Figure 2.

4.1. Geomorphology: Shoreline and Bathymetry

A total of 78 headlands were defined using USGS geological maps, remote-sensing imagery, NOAA navigational charts, and shoreline characterization geospatial databases from the California Coastal Sediment Management Workgroup (CSMW) (http://www.dbw.ca.gov/csmw/SpatialData.aspx, accessed 2013). The selection process for inclusion of a headland is as follows: 1) identification of a perturbation in the coastline in the remote-sensing imagery; 2) confirmation of a named headland in the navigational charts; 3) cross-confirmation as a distinct unit in the geological maps; and 4) identification of a change in shoreline characterization in the CSMW geospatial database. Criterion #2 preferentially selects headlands that are substantial in relative size because of their importance to navigation. At the base of each headland, a baseline was obtained by projecting a straight coastline that would exist in the absence of that headland (similar to low-pass filtering that separates the slowly curving coastline from the local perturbation due to the headland feature). Because of the asymmetrical nature of headlands, the 78 headlands represent 156 case studies for flow-topography interaction as flow patterns and sediment transport may be completely different for flow approaching the headland from one side versus the other.

A set of geometric parameters was extracted in ArcGIS (ESRI, 2013) based on the schematic displayed in Figure 3. These parameters were selected to quantify the size,

symmetry, and complexity of each headland and its relationship to the general trend of the coastline. If appropriate for a parameter, an "upstream" ('up') and "downstream" ('down') measurement was taken with upstream on the northerly or westerly side of a headland (i.e., on the right-hand side if looking out to sea) and downstream on the southerly or easterly side (i.e., left-hand side), based on the dominant direction of sediment transport in Southern California (Sallenger et al., 2002). For example, the angle of intersection between the shoreline of the headland and the baseline (ϕ) is expected to differ from one side to the other. Thus, measurements were obtained for both intersection points (ϕ_{up}, ϕ_{down}). Additional parameters were calculated from these measured parameters, including aspect ratio (width/length of headland), rugosity (baseline length/perimeter length), and combination of upstream and downstream angles at the apex of the headland. A summary of the measured and derived parameters is found in Table 1.

The underwater expression of a headland was determined by extracting bathymetry from merged data of the California Seafloor Mapping Program and California Shoreline Mapping Project (http://walrus.wr.usgs.gov/mapping/csmp/index.html). Five transects were plotted: three radiating transects locally normal to the shoreline of the headland and a shore-normal reference transect either side of the headland, where the shoreline is approximately straight and aligns with the baseline of the headland (Figure 4). The headland transects include upstream, center, and downstream transects (B, C, D) while the reference transects are only upstream and downstream (A, E). Bathymetry between 0 and 10 m was linearly interpolated and deeper depths were measured with advanced

bathymetric acoustic surveying. The distance from the shoreline to the 5, 10, 15, 20, 25, 30, 40, 50, and 75 m contours was tabulated along each of the five transects. Ratios were calculated between distances on a headland transect (e.g., X_{C10} where C denotes the center transect and 10 denotes distance to the 10 m isobath) and distances on a reference transect (e.g., X_{A10} referring to the distance to the 10 m isobath on the reference transect A); in this case the ratio $\chi_{10up} = X_{C10} / X_{A10}$. The downstream ratio would be $\chi_{10down} = X_{C10} / X_{E10}$. The median of χ along each transect was determined to yield simpler indicators of the bathymetric expression of the headland. Four ratios involving bathymetry were used to indicate whether an offshore ridge accompanies a headland. A ratio of one indicates that isobaths run parallel to the shoreline, curving offshore the same distance as the shoreline around the headland. If a ratio is greater than one, then the headland is more pronounced than the ridge (muted ridge), and vice versa –if the ratio is less than one, the ridge is amplified. The first ratio is the average for similar transect types (χ_{ave} = headland:reference). Ratios between the median of A and C (χ_{up}) and E and C (χ_{down}) were calculated to differentiate the upstream and downstream expression of the headland. Also, the ratio of the upstream to downstream median was calculated as an indicator of the bathymetric slope ratio (χ_m) between the two sides of the headland. In this ratio, the bathymetry off the headland is common, so it is comprised of ratios between X_A and X_E and the same measures for other isobaths – thus it represents the difference in offshore extent of shallow water (or nearshore bathymetric slope) from one side of the headland to the other.

4.2. Wave Climate

Waves are expected to dominate transport of sand past headlands. Storlazzi and Reid (2010) summarize the literature regarding wave-driven circulation and transport off central California. Modeled wave data were generated using the SWAN numerical model (Simulating WAves Nearshore, Holthuijsen et al. (1993); Booij et al. (1999); Ris et al. (1999)) to transform data on waves at outer shelf moorings to produce wave data for inner shelf locations (Erikson et al., 2014). Outer shelf wave data were obtained from the USACE Wave Information Studies (http://wis.usace.army.mil), based on 32 years of hourly hind-cast wave data (1984-2011). The same refraction-diffraction wave model was used to hindcast wave conditions for each headland in this study, yielding data for the 10 m isobath on the three headland transects (Figure 4). Monthly and seasonal means and 95-percentile values (high-energy events) were calculated for significant wave height (H_{sig}), peak period (T_p), and dominant direction (θ_d). Further, wave power (P), near-bed wave-orbital velocity (U_w), and wave-induced bed shear stress (τ) were calculated at the points according to methods of Soulsby (1997). Ratios of H_{sig} were also calculated to index the asymmetry of waves between upstream and downstream sides of each headland.

4.3. Database Pre-processing

The database consists of 50 parameters for each headland, yielding an extensive catalogue for data-mining techniques. Prior to analysis, the database was pre-processed to allow for direct comparison of the varied data types (discrete, continuous, and parameterized). In general, and specifically when using Euclidean distance as a clustering

tool, parameters require the same scale for an unbiased comparison. Thus data were standardized to rescale each parameter, which assumes the data exhibit a Gaussian distribution with representative mean and standard deviation values. Standardization produces a zero-mean and unit-variance for each parameter whereas normalization tends to overweight outliers and skew the remaining data toward low values.

The large multivariate database was reduced in size through correlation analysis using a threshold of R^2>0.70 to identify and remove parameters that are largely redundant with another parameter. The correlation analysis is key to simplify the extensive geomorphic and oceanographic parameters that were measured or derived. To aid interpretation, correlation analysis was chosen to retain selected measurable "real-world" variables instead of the orthogonal functions or principle components that would be generated using an EOF approach. For example, headland perimeter correlated with width (R^2=0.92, p<0.005), length (R^2=0.79, p<0.005), and area (R^2=0.90, p<0.005), allowing perimeter to represent all four parameters of "size". A correlation threshold value of 0.70 was selected as it achieves a high level of parameter reduction while maximizing the types of variables (i.e., size, shape, shoreline complexity, wave processes). The number of variables was reduced from 50 to 14 for the next stage of analysis. The initial 14 representative and 36 eliminated parameters are shown in Table 2.

4.4. Cluster Analysis

K-means clustering was selected for classification of headlands. *K*-means clustering is a simple, unsupervised learning algorithm that solves clustering problems (MacQueen, 1967). The procedure classifies a given data set into a certain number of clusters (selected

by user) and defines *K* centroids, one for each cluster. Through iteration, the centroids migrate to 1) minimize variability within clusters and 2) maximize variability between clusters. The minimization of the total intra-cluster variance, or the squared error function, *J* is

$$J = \sum_{j=1}^{k} \sum_{i=1}^{n} \left\| x_i^{(j)} - c_j \right\|^2 \quad (1)$$

where *k* is the number of clusters, *n* is the number of data point, $x_i^{(j)}$ is a data point at *i* for cluster *j* and c_j is the cluster center. In *K*-means clustering, the process moves objects (e.g., cases) in and out of clusters to get the most significant ANOVA (analysis of variance) results. Once the process is complete, the *F*-score for each parameter quantifies how much that parameter assists in defining a cluster. This data mining technique has been used in the oceanographic and coastal morphology sciences on wave climates (Camus et al., 2011), Pacific Ocean coral reefs (Freeman et al., 2012), and beaches (Scott et al., 2011).

The clustering process involved two rounds of iterations to refine the number of clusters and the types of parameters used. First, the subset of 14 parameters identified from the correlation analysis was used to perform clustering of 6-10 groups. As the wave climate variation along the coast from north to south was dominating over the geomorphic and bathymetric characteristics, the analyses were repeated with the four wave parameters removed to allow the 10 morphological parameters to drive the clustering. The wave parameters were not used for any further clustering analyses. The *F*-scores of parameters were reviewed to select the consistently highly rated parameters (Figure 5). The members of the clusters were cross-checked for sensible groupings (i.e., how similar were the mean

values and variance for the parameter? Is the combination of the shoreline and bathymetric data appropriate?). Eight clusters presented the preferred grouping. Second, the strength of each of the 10 parameters was tested by removing each one and re-running the eight clusters using the remaining nine parameters. In addition, cluster analysis was done using only parameters with F>5.0 and using only the three parameters with the highest F-scores. The mean of each cluster in these 12 additional cluster analyses was plotted using multi-dimensional scaling (MDS) to determine the similarity of the eight groups (Figure 6). The purpose of MDS is to provide a visual representation of the pattern of proximities (i.e., similarities or distances) among a set of objects (Kruskal, 1964; Kruskal and Wish, 1978). To assess the goodness-of-fit numerically and measure how well the visual configuration matches the data, a key evaluation factor is the stress test given as

$$S = \sqrt{\frac{\sum \sum (f(x_{ij}) - d_{ij})^2}{scale}} \tag{2}$$

where $f(x_{ij})$ is a function of the input data, d_{ij} is the Euclidean distance between i and j, and scale is a factor to maintain S ranging from 0 to 1. A stress of 0 shows perfect ordination. Scott et al. (2011) and Camus et al. (2011) used MDS to accompany the usage of K-means clustering in their classifications of beaches and wave climate, respectively. As seen in Figure 6, the "Top 3 F-scores" assortment of clusters produces the best spatial distribution in the MDS analysis; this assortment also produced a highly acceptable stress test value of S = 0.057. The final step to create the classes was to reverse the standardization and recover the actual values and units used for each parameter (i.e., return to a measured parameter with dimensions).

5. Results

5.1. Single-Parameter Distributions

The parameters could have been used individually to classify headlands (e.g., clustering exclusively based on aspect ratio). The distributions of the geomorphic-based 10 parameters across all headlands show variable structure (Figure 7). Most are unimodal (perimeter, aspect ratio, χ_{ave}, χ_{up}, χ_{down}, and χ_m); the remaining four are more evenly distributed (perimeter symmetry, coast curvature, coast intersection, and apex sharpness). The majority of the headlands are less than 5 km around, have lengths approximately twice the width (or amplitude), and have clear underwater expressions. The size distribution in particular shows the emphasis in this research on headlands that interrupt the nearshore flow and transport, not the shelf-scale circulation. The headlands' shorelines are also generally skewed upcoast although the largest category is the slight downcoast skewness. The shape of the headlands in terms of intersection with the coast and sharpness of the apex angle are less conclusive as individual clustering parameters. A multivariate approach to clustering was used instead to classify the headlands because multiple properties of headland shape are expected to influence flow and transport processes.

5.2. Morphological Classification

The three most important parameters in distinguishing the classes using morphological parameters are bathymetric slope ratio, size, and the sharpness of the headland's apex (α_{total}). If each parameter had three descriptive categories (e.g, small, medium, large or acute, balanced, obtuse), 27 hypothetical groups are possible. Classification allowed

identification of just eight clusters as preferred groupings after iterations, cross-checking and the 16 test analyses. These eight classes exhibit maximum similarity within each cluster and minimum similarity between clusters. The classes contain varying number of members (Table 3). For each class, the mean and standard deviation of distance from the center of the class are given as measures of the distribution of members within that class. Histograms of the three parameters show how the values distribute across the classes and for all classes combined (Figure 8). The following are summary descriptions of the eight classes, with individual headland details found in Appendix 1.

Type #1. Small size, mildly obtuse angle at apex, bathymetric symmetry; twenty-two headlands, constituting 28% of the database. This class is characterized by a mean perimeter size of 3.46 km ± 2.02 tightly grouped around the mean, a bathymetric slope ratio mean of 0.97 ± 0.37, and an apex angle mean of 107° ± 8.7. These headlands show slightly more underwater expression in the downstream direction (broader shallow region downstream). The range of apex angle is 90-120°, suggesting the headlands are neither strongly acute nor obtuse on the ocean-facing front. The headland closest to the cluster mean is El Jarro Point (Figure 9).

Type #2. Small size, slightly obtuse, strong downstream bathymetric expression; three headlands, constituting 4% of the database. This class is characterized by a mean perimeter size of 2.49 km ± 0.66, a bathymetric slope ratio mean of 3.55 ± 0.23, and an apex angle mean of 141° ± 17. These headlands are slightly obtuse on the ocean-facing front. The most distinguishing feature of this class is the strong downstream bathymetric

expression (deep nearshore waters downstream of headland), which is the second highest of all the classes. The three headlands are in Southern California, with Point La Jolla most representative (Figure 9).

Type #3. Mid-sized, obtuse, more downstream than upstream bathymetric expression; twelve headlands, constituting 15% of the database. This class is characterized by a mean perimeter size of 5.21 km ± 2.3, a bathymetric slope ratio mean of 1.56 ± 0.4, and an apex angle mean of 142° ± 13. These headlands are fairly obtuse and have more of a downstream underwater expression than upstream. Horseshoe Point is closest to the mean of the class (Figure 9).

Type #4. Mid-sized, obtuse, extreme downstream bathymetric expression; a single headland, Point Loma, constituting 1% of the database (Figure 9). This headland has a perimeter size of 5.41 km, a bathymetric slope ratio of 6.17, and an apex angle of 116°. The extreme imbalance of the bathymetric slope ratio is due to the geography of Point. Loma at the entrance to San Diego Bay to the east of the headland. For the other two parameters, this class is very similar to Type #3 and would be included in that group if not for the bathymetric slope ratio.

Type #5. Small sized, acute, upstream bathymetric expression; ten headlands, constituting 13% of the database. This class is characterized by a mean perimeter size of 3.99 km ± 1.87, a bathymetric slope ratio mean of 1.13 ± 0.37, and an apex angle mean of 108° ± 8.0. Point Sierra Nevada is representative of this class (Figure 9).

Type #6. Small size, obtuse, upstream bathymetric expression; twenty headlands, constituting 26% of the database. This class is characterized by a mean perimeter size of 1.74 km ± 1.16, a bathymetric slope ratio mean of 0.97 ± 0.23, and an apex angle mean of 151° ± 12. This large group contains the two tombolos in the database – Goat Rock and Morro Rock. Despite the appearance of very different headlands, the overall mean distance for the group is 0.26 ± 0.10 (tighter than most clusters). Bolsa Point is a good representative (Figure 9).

Type #7. Large size, acute, balanced bathymetric expression; five headlands, constituting 6% of the database. This class is characterized by a mean perimeter size of 13.77 km ± 2.2, a bathymetric slope ratio mean of 1.03 ± 0.56, and an apex angle mean of 77° ± 20. These headlands are sharply acute and have a balanced underwater expression. Picking a representative for this class is more challenging than the others because they are large enough to contain small, unidentified headlands. Point Arena shows several characteristics of a large headland with sharp points protruding well past the width of the surf zone but generally represents this class well (Figure 9).

Type #8. Largest size, obtuse, balanced bathymetric expression; five headlands, constituting 6% of the database. This class is characterized by a mean perimeter size of 23.35 km ± 6.87, a bathymetric slope ratio mean of 1.23 ± 0.8, and an apex angle mean of 162° ± 13. These headlands are the largest in the database, broad faced, and have a balanced underwater expression. This group includes the mega-headland of Monterey

Peninsula. They show complex shorelines with several smaller headlands, some of which have been identified in the other headland types. The representative for this class is Patrick's Point/Trinidad Head, which has a compound shoreline (Figure 9).

The eight types of headland classes described above create the best possible arrangement using the three most important parameters based on the clustering analysis. The morphologically-based headland classes provide a sorting of California headlands to perform analysis of flow regimes, wave interactions, and littoral cell boundaries specific to each class.

6. Discussion

6.1. Classes of Headlands and Key Parameters

The process used to classify the 78 California headlands sought to merge easily measured shoreline and bathymetric parameters into a large database for cluster analysis. Several of the basic parameters (size, shape, shoreline complexity) suggested clusters, but as the analysis proceeded, many of the simplest parameters did not exert as much influence as were initially expected. For example, aspect ratio appears to be a characteristic of a headland that can affect an alongshore jet (Signell and Geyer, 1991) or sea stack-headland evolution (Limber and Murray, 2015). However, this parameter does not play a primary role in defining clusters – it had a low *F*-score, indicating that it had limited skill in differentiating between headlands (i.e., most headlands exhibit similar aspect ratios). The iterative sequence of removing parameters and rerunning the clustering and MDS

analyses proved that the most distinct classes emerge when only the top three *F*-scoring parameters are used.

Based on the use of perimeter, bathymetric slope ratio, and apex angle, the headlands fell into eight distinctive clusters, with only one member of Type 4 (Point Loma), which could be considered an outlier – leaving just 7 classes: 4 classes of small headlands, 1 mid-size class and 2 classes of big headlands (one class with acute angles and the other with obtuse angles). The MDS plot (Figure 10) shows that Types 1, 3, 5, and 6 are similar, and distinction between classes may depend on which parameters are used in the analysis (Figure 6). Relative to that group of clusters, Types 7 and 8 are distinct (the two big headland classes), and also Types 2 and 4 are distinct (both characterized by acute angles and deep waters downstream of the headland).

The importance of the three primary parameters may be interpreted in terms of flow and wave processes. For example, the size of the headland is critical relative to the width of wave action, and the apex sharpness is important for flow separation and eddy generation. The change in bathymetry from one side of the headland to the other irrespective of the details of the headland can also be key to flow separation and offshore export of sediment: deep water downstream is more likely to yield an offshore loss of sand and a break in the continuity of longshore transport – this parameter emerges below as the most important in identifying headlands that align with littoral cell boundaries.

This first-of-its-kind classification does not come without areas for improvement to either the method or the data itself. For the headland classes, three revisions could be considered to enhance the results. First, whereas 78 headlands is a sizable number, the California coast is 1,800 km long and several potential entries to the database were excluded due to not satisfying the criteria detailed in Section 4. A different set of parameters to delineate headlands may produce a larger database. Second, offshore reefs and sea stacks were not included in the boundary of a headland due to lack of data. Some of these features, particularly the reefs, were likely resolved in the bathymetry, but the overall sizes of the headlands could be larger than when defined by the shoreline. Hence the size parameters (*L*, *W*, perimeter, and area) may be underestimated. Last, the bedrock geology offshore could have an additional control on the clusters or at least correlate with some of the geomorphic parameters. Stul et al. (2012) were able to incorporate geology more explicitly than this study, which suggests headlands and littoral cell boundaries may be better understood when the lithology and resistance to erosion are considered. Examining any or all of the preceding could test the efficacy of the current classifications.

6.2. Wave-Driven Transport Past Headlands

These headland classes provide a descriptive grouping of similar sizes, shapes, and shoreline complexities – classes determined by morphological similarity, without any information on waves, or sediment transport. Given that the role of wave energy in circulation and sediment transport around headlands is critical (Davies, 1974; Hume et al., 2000; Pattiaratchi et al., 1987), a brief exploration of how waves interact with headlands was conducted to demonstrate an application of the headland classes. From

wave data at 10 m on each of the three headland transects, the angle between waves and shore-normal was determined as a measure of longshore transport for the 78 headlands. Without determining power and without estimating the sediment flux (Kamphuis, 2010), it is possible to identify when longshore transport is continuous around the headland or when it is in opposite directions on either side of the headland, indicating a discontinuity in wave-driven transport past the headland. The transport for the 78 headlands was characterized for winter and summer mean and 95-percentile conditions as one of four possibilities: continuous upcoast, continuous downcoast, convergent, or divergent (Figure 11).

The results by headland class show that the geomorphically-based clusters translate well to wave-driven transport scenarios. Only headland Type 4 (Point Loma) is discontinuous under all conditions – likely to always block wave-driven transport. Headland Type 2 is also often divergent, with continuous transport occurring at times, but only downcoast. Type 8 is similar to Type 2, but transport is blocked less often (size seems less important than asymmetry). At Type 7 headlands, wave-driven transport is blocked more often, but upcoast transport can also occur in winter. At other headlands (the central grouping of clusters: 1, 3, 5 and 6), continuous transport past the headland is common for mean and 95-percentile conditions and both upcoast and downcoast transport can occur. While 95-percentile conditions are most important because transport will occur during high-energy events, there are only small differences between incident directions for mean and high-energy conditions. There is seasonality for all types other than Types 2 and 4, as expected and consistent with the ideas put forward by van Rijn (2010). The seasonal shifts between

continuous or blocked transport is supported by the work in Australia by Stul et al. (2012) and Goodwin et al. (2013), which suggest that headland transport can effectively turn 'on' or 'off' seasonally.

6.3. Littoral Cell Boundaries in California

The 27 headlands identified by Habel and Armstrong (1978) as littoral cell boundaries can be related to the headland classes to determine if certain geomorphic and/or bathymetric parameters may clarify a headland's role in blocking sediment transport. Table 3 shows that all of the headlands of Type 4 and Type 2 are littoral cell boundaries and both are characterized by marked bathymetric slope ratios, with steep slopes and deep water downstream when flow is southward. Type 8 (biggest headlands) has 4 out of 5 headlands acting as boundaries and Type 7 has 3 out of 5 (big headlands, smaller than Type 8, but with acute apex). The other headland types (1, 3, 5, 6) have less than a third of their members acting as boundaries (Table 3). This is consistent with the analyses presented in Figure 11 where Types 2, 4, 7, and 8 typically experience being divergent or convergent for wave-driven transport. Based on these results, big headlands and headlands with deep water downstream (and acute apexes) are effective littoral cell boundaries. While those headland types are likely to act as littoral cell boundaries, the relationship between type and boundary is not entirely convincing. Fourteen of the 27 littoral cell boundary headlands fall into headland classes that are not typically boundaries. For example, one boundary falls into Type 5, which is characterized by small sizes and obtuse apexes – headlands that may be easily enveloped and by-passed by alongshore currents.

The seasonal wave power is shown alongside transport direction in Figure 12. Winter wave power is larger than in summer for almost all of the headlands, regardless of headland type. Seasonal variability in wave power and transport direction is evident with some headlands turning transport 'on' in winter conditions (e.g., Bolinas Point) while others become barriers to transport (e.g., Bruhel Point). Members of Type 6 headlands are the most seasonally variable of all the boundary headlands while those in Types 2, 3, 4, 7 are consistent across the seasons. The littoral cell boundary headlands can be sorted into two categories: those that do not change seasonally, and those that change seasonally. The 20 non-seasonal headlands include 9 headlands for which wave transport is continuous and in a consistent direction both winter and summer and 11 headlands for which wave transport is discontinuous. The wave-driven transport past the remaining 7 headlands changes seasonally, with 6 becoming a boundary seasonally and one Type 6 headland experiencing reversed transport seasonally.

The association of some littoral cell boundaries with headland classes that are not likely to block sediment transport may be explained by inadequacies in headland clustering, indexing of continuity of wave-driven transport past headlands, or definition of the boundaries of littoral cells. Inadequacy in headland clustering may be due to omission of a key morphological factor or problems with the clustering approach. This seems unlikely given the routine use of *K*-means clustering and the comprehensive initial list of parameters. The second possibility is that a simple wave-direction analysis does not properly capture the likelihood of continuous/blocked transport. High-resolution numerical modeling in a subsequent analysis could elucidate this point. Notwithstanding

inadequacies in clustering or indexing of transport, the findings suggest significant inadequacies in the definition of littoral cell boundaries – specifically those that align with small/mid-sized headlands without acute apexes or deep water downstream (i.e., Types 1, 3, 5, 6).

The conclusions above show that a better definition of littoral cell boundary is required and a recognition that while some boundaries may be close to perfect obstacles, others are weak and variable with significant leakage. Stul et al. (2012) described littoral cells as tiered according to primary, secondary, and tertiary levels along the coast of Western Australia with sediment exchange possible among the lower levels. California's littoral cells as defined by Habel and Armstrong (1978) do not contain subcells, but Patsch and Griggs (2007) expanded some of the cells to create compound cells (e.g., Santa Monica). Other cells defined by Habel and Armstrong (1978) are in such close proximity that the divisions could be arbitrary, such as near the mouth of the San Francisco Bay where the Bolinas Bay and San Francisco cells are adjacent to each other. Further, the method used by Habel and Armstrong (1978) to delineate the boundaries was not explicitly described, so the factors they used are ambiguous. This contrasts with the bathymetry, topography, remote sensing imagery, historic coastal change, shoreline position, sediment information, dunes, and geological maps that were compiled by Stul et al. (2012) to create the Western Australia boundaries. Redefining littoral cell boundaries for California is beyond the scope of this paper, but clearly a need for the region.

7. Conclusion

California headlands were grouped into eight classes that represent distinct headland types in terms of geomorphic and bathymetric parameters. Headland perimeter, apex sharpness, and bathymetric slope ratio were found to exert the most control on classifying the 78 headlands along the California coast. Hindcast wave data were used to investigate the likelihood of continuous sediment transport around the headland and determine the efficacy of the headland as a littoral cell boundary. Headlands characterized by large size, deep water downstream and acute apex angles were shown to result in low likelihood of wave-driven transport past the headland. Most of these headlands aligned with littoral cell boundaries. However, many littoral cell boundaries aligned with headlands that did not fall into these classes, raising questions about the efficacy of these headlands in blocking alongshore transport. Based on these findings, the traditional California littoral cell boundaries are questionable and an in-depth analysis is needed.

Acknowledgments

This work was supported by the Hydrologic Sciences Graduate Group at the University of California Davis and by the US Geological Survey's Coastal and Marine Geology program. The authors wish to thank Elena Vandebroek (Delft), Dennis Hall (NOAA), and Dewberry for providing geospatial technical assistance and data and Li Erikson (USGS) for providing wave data for the paper. Discussions regarding geomorphology with Rocko Brown (UCD) and cluster analysis with Christie Hegermiller (UCSC) helped guide this research. The manuscript was improved by review from Bruce Jaffe (USGS), Edward Thornton (NPS), and an anonymous review. Use of trademark names does not suggest USGS endorsement of products.

Tables

Table 1. Measured and Derived Parameters and Exploratory Ratios for Headlands Classification

Category	Measured Parameters	Derived Parameters	Exploratory Ratios
Geomorphology	Width (W) Length (L) Perimeter Area Curvature of Coast (θ) Inside Angle of Headland-Coast Intersection (ϕ_{up}, ϕ_{down}) Angle of Headland Apex (α_{up}, α_{down})	Perimeter Symmetry Difference in Upstream-Downstream Angle ($\Delta\phi$) Apex Sharpness (α_{total})	• Aspect Ratio (W/L) • Rugosity (Perimeter/L)
Bathymetry	Cross-shore Distance to Contours* for 3 Radiating Headland Normal Transects ($x_{*hdlnd\_up/ctr/dn}$) Cross-shore Distance to Contours* for 2 Shore Normal Transects ($x_{*normal\_up/dn}$)	Median of Distance for Each Headland Transect ($x_{hdlnd\_up/ctr/dn}$) Mean of Median Distances for the Headland Transects (x_{hdlnd_ave}) Median of Distance for Each Reference Transect ($x_{reference\_up/dn}$) Mean of Median Distances for the Reference Transects ($x_{reference\_ave}$)	• Ratio of Means ($\chi_{ave} = x_{hdlnd\_ave}/x_{reference\_ave}$) • Ratio of Upstream Transects ($\chi_{up} = x_{hdlnd\_ctr}/x_{normal\_up}$) • Ratio of Downstream Transects ($\chi_{down} = x_{hdlnd\_ctr}/x_{normal\_down}$) • Bathymetric Slope Ratio (χ_m = Upstream/ Downstream)
Oceanography	Wave Climate at 3 Points per Headland (seasonal, mean and top 5% extreme events) • Significant Wave Height (H_{sig}) • Peak Period (T_p) • Dominant Direction (θ_d)	Wave-driven Transport at 3 Points per Headland and Mean per Headland • Wave power (P) • Bottom orbital velocities (U_w) • Bottom shear stress (τ) Mean H_{sig}, P, U_w, τ for Headland in Winter and Summer Mean and Top 5% Conditions	• Ratio of Wave and Transport Parameters between Upstream and Downstream Points by Season and Event (e.g., Winter Mean $H_{sig\_upWM}/H_{sig\_downWM}$)

* - Contour depths: 5, 10, 15, 20, 25, 30, 40, 50, and 75 m

Table 2. Correlated Parameters for Variable Reduction

Representative Parameter	Eliminated Parameters	R^2 (all p<0.005)
Perimeter	Width	0.92
	Length	0.79
	Area	0.90
Aspect Ratio	Rugosity	-0.70
Perimeter Symmetry	None	-
Curvature of Coast (θ)	None	-
Difference in Upstream-Downstream Angle ($\Delta\phi$)	ϕ_{up}	0.73
	ϕ_{down}	-0.72
Apex Sharpness (α_{total})	α_{up}	0.85
	α_{down}	0.77
Ratio of Means (χ_{ave})	None	-
Ratio of Upstream Transects (χ_{up})	None	-
Ratio of Downstream Transects (χ_{down})	None	-
Bathymetric Slope Ratio (χ_m)	None	-
Mean H_{sig} in Winter Mean Conditions	Top 5% Winter H_{sig}	0.91
	Top 5% Winter P	0.85
	Top 5% Winter U_w	0.90
	Top 5% Winter τ	0.90
	Mean Winter P	0.95
	Mean Winter U_w	0.83
	Mean Winter τ	0.77
Ratio of H_{sig} between Upstream and Downstream Points in Winter Mean Conditions ($H_{sig\_upWM}/H_{sig\_downWM}$)	Top 5% Winter H_{sig} Ratio	0.85
	Top 5% Winter P Ratio	0.70
	Top 5% Winter U_w Ratio	0.74
	Top 5% Winter τ Ratio	0.72
	Mean Winter P Ratio	0.78
	Mean Winter U_w Ratio	0.70
	Mean Winter τ Ratio	0.70
Mean H_{sig} in Summer Mean Conditions	Top 5% Summer H_{sig}	0.98
	Top 5% Summer P	0.91
	Top 5% Summer U_w	0.86
	Top 5% Summer τ	0.80
	Mean Summer P	0.94
	Mean Summer U_w	0.77
	Mean Summer τ	0.70
Ratio of H_{sig} between Upstream and Downstream Points in Summer Mean Conditions ($H_{sig\_upSM}/H_{sig\_downSM}$)	Top 5% Summer H_{sig} Ratio	0.98
	Top 5% Summer P Ratio	0.82
	Top 5% Summer U_w Ratio	0.74
	Top 5% Summer τ Ratio	0.76
	Mean Summer P Ratio	0.90
	Mean Summer U_w Ratio	0.70
	Mean Summer τ Ratio	0.71

Table 3. Headland Classes after Clustering and California Littoral Cell Comparison

Headland Class	Number of Members	Percent of Database (%)	Distance from Cluster Center	Perimeter (mean km)	(description)	Bathymetric Slope Ratio (mean)	(description)	Apex Sharpness (mean °)	(description)	Littoral Cell Boundary[1]
1	22	28.2	0.31±0.15	3.46±2.02	Small	0.97±0.37	Upstream	107±8.7	Mildly obtuse	4 (18%)
2	3	3.8	0.26±0.14	2.49±0.66	Small	3.55±0.23	Downstream	141±17	Obtuse	3 (100%)
3	12	15.4	0.39±0.12	5.21±2.30	Small-medium	1.56±0.40	Downstream	142±13	Obtuse	3 (25%)
4	1	1.3	--	5.41	Small-medium	6.17	Extreme downstream	116	Obtuse	1 (100%)
5	10	12.8	0.32±0.14	3.99±1.87	Small	1.13±0.37	Downstream	108±8.0	Mildly obtuse	1 (10%)
6	20	25.6	0.26±0.10	1.74±1.16	Small	0.97±0.23	Upstream	151±12	Obtuse	6 (30%)
7	5	6.4	0.49±0.14	13.77±2.20	Large-medium	1.03±0.56	Balanced	77±20	Acute	3 (60%)
8	5	6.4	0.73±0.35	23.35±6.87	Large	1.23±0.80	Downstream	162±13	Very obtuse	4 (80%)
All	78	100	0.35±0.21	7.30±7.13		2.08±1.87		128±28		25

1 Percent of class members defined as a littoral cell boundary by Habel and Armstrong (1978)

Figure Captions

Figure 1. Overview of California study area with major bays, peninsulas, and promontories noted.

Figure 2. Flow diagram illustrating the process for assembly and analysis of morphological and wave data to produce a headland classification scheme.

Figure 3. Schematics of geometric and geomorphic parameters used in analysis of California headlands.

Figure 4. Schematic of bathymetry used to characterize the underwater expression of a headland. Relevant bathymetric blocks were extracted from merged data of the California Seafloor Mapping Program and California Shoreline Mapping Project. The darker gray shaded portion is the defined headland. Bathymetric contours for depths of 5, 10, 15, 20, 25, 30, 40, 50, and 75 m are shown. Lines B, C and D are the "headland" transects and lines A and E are the "reference" transects. The distance from shore to the contours was tabulated along the five transects for all headlands.

Figure 5. *F*-values for the morphological parameters evaluated for analyses producing different numbers of clusters: perimeter, perimeter symmetry of headland, aspect ratio of width/length, curvature of coast at the headland, difference between the upstream and downstream intersection of the headland and coastline, apex angle, mean of median transects ratio, and the bathymetric slope ratio between the upstream and downstream

underwater expression of the headland. Perimeter, apex angle, and bathymetric slope ratio scored consistently higher than the other parameters in influencing the clustering.

Figure 6. Investigation of the influence of each parameter on the clustering algorithm for eight clusters using multi-dimensional scaling (MDS) analysis. Each parameter was removed from the K-means clustering process and the mean of the eight clusters was plotted. Two other cluster analyses were also used: the top three F-scoring parameters and any parameter with F>5.0. Based on the MDS plot, the top three F-scoring parameters of perimeter, bathymetric slope ratio, and sharpness of headland apex produce the most distinct eight clusters.

Figure 7. Histograms for the distribution of values for the 10 geomorphic parameters used in the cluster analysis.

Figure 8. Histograms for the distribution of values for the top three parameters responsible for cluster generation by class (first 8 columns) and for all classes combined (last column). Top row: Perimeter (km). Middle row: Bathymetric slope ratio. Bottom row: Apex angle α (degrees). Vertical axis scale expands for the last column. Horizontal scales for perimeter and angle are linear, and logarithmic for ratio.

Figure 9. Representative headlands for each class. 1) Point El Jarro, 2) Point La Jolla, 3) Horseshoe Point, 4) Point Loma, 5) Point Sierra Nevada, 6) Bolsa Point, 7) Point Arena, and 8) Patrick's Point/Trinidad Head. Red polygons delineate the headland extent as

defined using remote-sensing imagery, geological maps, navigational charts, and shoreline characterization data.

Figure 10. Multi-dimensional scaling (MDS) plot and the means of the three parameters responsible for cluster generation. The variability around each mean is one standard deviation. Top left: MDS relationship among the classes and size of class. Bottom left: Perimeter (km). Top right: Bathymetric slope ratio. The dotted line signifies a ratio of 1. Bottom right: Headland apex angle, α (degrees).

Figure 11. Portion of transport possibilities (upcoast, downcoast, convergent, and divergent) for each headland class under four wave conditions (a - winter, 95-percentile, b - winter, mean, c - summer, 95-percentile, and d - summer, mean). Each class size is normalized. Upcoast and downcoast transport is continuous around the headland, so that it will not block sediment transport, while convergent and divergent transport will not allow transport around the headland.

Figure 12. Average wave power (kW/m) and transport direction in winter and summer mean (solid dots) and 95-percentile (open dots) conditions for the 27 California headlands used to define the traditional California littoral cell boundaries. The headlands are grouped by class type. Winter conditions generate larger wave power than summer for all headlands. Convergent and divergent transport directions are considered barriers to alongshore transport and can produce *permanent* boundaries (e.g., Types 4 and 7). Seasonal shifts in transport direction produce *seasonal* boundaries (e.g., some headlands in Type 6). See Table 3 for portion of littoral cell boundary headlands within a class.

Appendix 1

Classified Headland Database with Key Geomorphic Clustering Parameters
Italicized Headland Name Indicates Littoral Cell Boundary (Habel and Armstrong, 1978)

Headland Id	Headland	Headland Class	Perimeter (km)	Apex Sharpness (α,°)	Bathymetric Slope Ratio
1	*Pt. St. George*	8	18.27	164.8	0.624
2	*Trinidad Head/Patricks Point*	8	20.27	172.4	1.086
3	*False Cape*	1	1.76	114.9	1.146
4	*Cape Mendocino*	6	2.11	136.0	0.663
5	*Punta Gorda*	3	6.49	142.6	0.970
6	*Pt. Delgada*	3	6.93	147.7	1.074
7	Cape Vizcaino	1	3.75	111.2	1.216
8	*Bruhel Pt*	6	3.98	155.4	0.673
9	*Laguna Pt*	1	2.30	101.4	0.767
10	*Pt Arena*	7	16.21	54.9	0.649
11	Havens Neck	1	2.70	100.6	0.611
12	Black Pt	5	4.94	82.6	1.083
13	Horseshoe Pt	3	5.61	143.7	1.381
14	Salt Pt	1	4.64	96.4	0.578
15	*Fort Ross*	6	1.71	139.3	0.962
16	Goat Rock	6	0.85	146.6	0.774
17	*Bodega Head*	8	16.01	174.1	1.570
18	*Pt Reyes*	8	23.60	143.7	2.418
19	*Double Pt*	1	2.39	117.1	1.196
20	*Bolinas Pt*	6	1.60	137.5	1.067
21	*Duxbury Pt*	3	3.16	128.2	1.355
22	Rocky Pt	1	1.06	99.6	0.108
23	Pt Bonita	5	4.79	81.6	0.349
24	Mussel Rock	6	1.19	167.4	0.932
25	Mori Pt	6	0.59	149.1	0.942
26	Rockaway	6	0.84	145.5	0.998
27	*Pt San Pedro*	1	2.89	97.4	0.467
28	*Pillar Pt*	3	3.06	125.2	2.087
29	Bolsa Pt	6	2.45	153.6	0.861
30	Pigeon Pt	5	2.59	76.5	1.354
31	Franklin Pt	3	4.11	167.5	1.500
32	Ano Nuevo	1	7.33	110.6	0.783
33	El Jarro Pt	1	2.28	109.2	1.014
34	Pt Santa Cruz	5	2.44	53.4	2.346
35	Cabrillo Pt	6	0.70	143.2	1.270
36	Lovers Pt	6	0.58	155.3	1.143
37	*Pt Pinos*	6	4.34	147.5	0.965

38	Pt Joe	6	1.49	150.9	0.674
39	Cypress	3	10.20	129.2	1.258
40	Pt/Pescadero Pt Monterey	8	33.59	154.4	0.441
41	Peninsula *Pt Lobos*	7	13.75	56.1	1.877
42	Yankee Pt	1	3.15	112.9	0.730
43	*Castle Pt*	1	2.46	105.5	1.220
44	Hurricane Pt	1	3.41	123.9	1.067
45	Pt Sur	3	4.48	137.7	2.061
46	Cooper/Pfeiffer Pt	1	8.37	126.0	0.452
47	Gamboa Pt	5	0.93	72.8	0.838
48	Lopez Pt	6	1.62	171.8	1.386
49	Salmon Cone	6	0.66	138.9	0.766
50	Ragged Pt	3	2.37	128.9	1.406
51	*Pt Sierra Nevada*	5	1.51	73.8	0.909
52	Pt Piedras Blancas	6	3.86	163.5	0.690
53	San Simeon Pt	1	3.05	100.4	1.227
54	Estero Pt	1	2.49	99.9	1.600
55	Cayucos Pt	1	2.40	107.0	1.225
56	Morro Rock	6	2.27	174.1	0.965
57	*Pt Buchon*	7	10.51	88.0	0.512
58	Pt San Luis	3	7.70	146.5	2.011
59	Pt Sal	1	6.75	108.2	1.023
60	Purisma Pt	1	1.63	107.7	0.899
61	Pt Penderales	5	2.23	57.6	0.990
62	Pt Arguello	7	13.08	97.7	0.816
63	Pt Conception	5	1.98	74.6	0.637
64	Government Pt	1	2.55	108.0	1.141
65	Coal Oil Pt/Goleta Pt	1	6.82	93.7	1.465
66	Santa Barbara Pt	3	5.16	159.6	2.091
67	Rincon Pt	1	1.88	117.2	1.410
68	Pitas Pt	3	3.29	145.0	1.533
69	Pt Mugu	6	0.63	153.8	1.087
70	Pt Dume	7	15.29	90.4	1.298
71	*Palos Verdes Pt*	6	1.50	128.8	1.135
72	Pt Vicente	5	0.95	88.0	0.938
73	Long Pt	6	1.80	162.3	1.406
74	*Pt Fermin*	2	3.00	159.1	3.376
75	Abalone Pt	5	1.43	57.4	0.857
76	*Dana Pt*	2	1.75	138.0	3.468
77	*Pt La Jolla*	2	2.71	125.5	3.818
78	*Pt Loma*	4	5.41	116.6	6.173

8. REFERENCES

Alaee, M.J., Ivey, G., Pattiaratchi, C., 2004. Secondary circulation induced by flow curvature and Coriolis effects around headlands and islands. Ocean Dynamics 54, 27-38.
Backstrom, J.T., Jackson, D.W.T., Cooper, J.A.G., 2009. Mesoscale shoreface morphodynamics on a high-energy regressive coast. Continental Shelf Research 29, 1361-1372.
Barnard, P.L., Hansen, J.E., Erikson, L.H., 2012. Synthesis Study of an Erosion Hot Spot, Ocean Beach, California. Journal of Coastal Research 28, 903-922.
Bastos, A.C., Kenyon, N.H., Collins, M., 2002. Sedimentary processes, bedforms and facies, associated with a coastal, headland: Portland Bill, Southern UK. Marine Geology 187, 235-258.
Best, T.C., Griggs, G.B., 1991. The Santa-Cruz Littoral Cell - Difficulties in Quantifying a Coastal Sediment Budget.
Booij, N., Ris, R.C., Holthuijsen, L.H., 1999. A third-generation wave model for coastal regions - 1. Model description and validation. Journal of Geophysical Research-Oceans 104, 7649-7666.
Camus, P., Mendez, F.J., Medina, R., Cofino, A.S., 2011. Analysis of clustering and selection algorithms for the study of multivariate wave climate. Coastal Engineering 58, 453-462.
CGS, 2002. California Geomorphic Provinces. California Geological Survey, California Department of Conservation, p. Note 36.
CGS, 2006. California Geological Map, Map Series 57 ed. California Geological Survey, California Department of Conservation.
Chadwick, D.B., Largier, J.L., 1999. Tidal exchange at the bay-ocean boundary. Journal of Geophysical Research-Oceans 104, 29901-29924.
Collen, J.D., Gardner, J.P.A., Garton, D.W., 2009. Application of the littoral cell concept to managing a protected atoll: Palmyra Atoll National Wildlife Refuge. Ocean & Coastal Management 52, 628-635.
Cooper, N.J., Pontee, N.I., 2006. Appraisal and evolution of the littoral 'sediment cell' concept in applied coastal management: Experiences from England and Wales. Ocean & Coastal Management 49, 498-510.
Covault, J.A., Normark, W.R., Romans, B.W., Graham, S.A., 2007. Highstand fans in the California borderland: The overlooked deep-water depositional systems. Geology 35, 783-786.
Dai, Z.J., Liu, J.T., Lei, Y.P., Zhang, X.L., 2010. Patterns of Sediment Transport Pathways on a Headland Bay Beach-Nanwan Beach, South China: A Case Study. Journal of Coastal Research 26, 1096-1103.
Davies, J.L., 1974. The coastal sediment compartment. Australian Geographical Studies 12, 139-151.
Davies, P.A., Dakin, J.M., Falconer, R.A., 1995. Eddy Formation Behind a Coastal Headland. Journal of Coastal Research 11, 154-167.
de Castilhos, J.A., Gre, J.C.R., 2006. Beach morphodynamics and sediment transport along the northern coast of Santa Catarina, Brazil. Journal of Coastal Research, 1756-1761.

Denniss, T., Middleton, J.H., Manasseh, R., 1995. Recirculation in the Lee of Complicated Headlands - A Case-Study of Bass-Point. Journal of Geophysical Research-Oceans 100, 16087-16101.
Drake, P.T., McManus, M.A., Storlazzi, C.D., 2005. Local wind forcing of the Monterey Bay area inner shelf. Continental Shelf Research 25, 397-417.
Emery, K.O., Kuhn, G.G., 1982. Sea cliffs: Their processes, profiles, and classification. Geological Society of America Bulletin 93, 644-654.
Erikson, L.H., Storlazzi, C.D., Golden, N.E., 2014. Modeling Wave and Seabed Energetics on the California Continental Shelf. Pamphlet to accompany data set., in: Survey, U.S.G. (Ed.), Santa Cruz, California.
Erikson, L.H., Wright, S.A., Elias, E., Hanes, D.M., Schoellhamer, D.H., Largier, J., 2013. The use of modeling and suspended sediment concentration measurements for quantifying net suspended sediment transport through a large tidally dominated inlet. Marine Geology 345, 96-112.
ESRI, 2013. ArcGIS Desktop: Release 10.1 Environmental Systems Resource Institute, Redlands, CA.
Everts, C.H., Eldon, C.D., 2000. Beach-Retention Structures and Wide Sandy Beaches in Southern California. Shore and Beach 68, 11-22.
Freeman, L.A., Miller, A.J., Norris, R.D., Smith, J.E., 2012. Classification of remote Pacific coral reefs by physical oceanographic environment. Journal of Geophysical Research-Oceans 117.
Goodwin, I.D., Freeman, R., Blackmore, K., 2013. An insight into headland sand bypassing and wave climate. variability from shoreface bathymetric change at Byron Bay, New South Wales, Australia. Marine Geology 341, 29-45.
Guillou, N., Chapalain, G., 2011. Effects of waves on the initiation of headland-associated sandbanks. Continental Shelf Research 31, 1202-1213.
Habel, J.S., Armstrong, G.A., 1978. Assessment and Atlas of Shoreline Erosion Along the California Coast. State of California, Department of Navigation and Ocean Development, Sacramento, CA, p. 277.
Harris, P.T., Whiteway, T., 2011. Global distribution of large submarine canyons: Geomorphic differences between active and passive continental margins. Marine Geology 285, 69-86.
Holthuijsen, L.H., Booij, N., Ris, R.C., 1993. A spectral wave model for the coastal zone, Proceedings of the 2nd International Symposium on Ocean Wave Measurement and Analysis,, New Orleans, pp. 630-641.
Hume, T.M., Oldman, J.W., Black, K.P., 2000. Sediment facies and pathways of sand transport about a large deep water headland, Cape Rodney, New Zealand. New Zealand Journal of Marine and Freshwater Research 34, 695-717.
Inman, D.L., Frautschy, J.D., 1966. Littoral processes and the development of shorelines, Coastal Engineering Special Conference. ASCE, pp. 511-536.
Jones, O.P., Simons, R.R., Jones, E.J.W., Harris, J.M., 2006. Influence of seabed slope and Coriolis effects on the development of sandbanks near headlands. Journal of Geophysical Research-Oceans 111.
Kamphuis, J.W., 2010. Introduction to coastal engineering and management, 2nd Edition. World Scientific, Singapore.

Kaplan, D.M., Halle, C., Paduan, J., Largier, J.L., 2009. Surface currents during anomalous upwelling seasons off central California. Journal of Geophysical Research 114.
Kruskal, J.B., 1964. Multidimensional-Scaling by Optimizing Goodness of Fit to a Nonmetric Hypothesis. Psychometrika 29, 1-27.
Kruskal, J.B., Wish, M., 1978. Multidimensional Scaling. SAGE Publications.
Largier, J.L., Magnell, B.A., Winant, C.D., 1993. Subtidal Circulation over the Northern California Shelf. Journal of Geophysical Research-Oceans 98, 18147-18179.
Limber, P.W., Murray, A.B., 2015. Sea stack formation and the role of abrasion on beach-mantled headlands. Earth Surface Processes and Landforms 40, 559-568.
Limber, P.W., Patsch, K.B., Griggs, G.B., 2008. Coastal sediment budgets and the littoral cutoff diameter: A grain size threshold for quantifying active sediment inputs. Journal of Coastal Research 24, 122-133.
Loureiro, C., Ferreira, O., Cooper, J.A.G., 2012. Geologically constrained morphological variability and boundary effects on embayed beaches. Marine Geology 329, 1-15.
MacQueen, J.B., 1967. Some Methods for Classification and Analysis of Multivariate Observations, 5th Berkeley Symposium on Mathematical Statistics and Probability. University of California Press, Berkeley, California, pp. 281-297.
Milliman, J.D., Farnsworth, K.L., 2011. River Discharge to the Coastal Ocean: A Global Synthesis. Cambridge University Press, New York.
Mullenbach, B.L., Nittrouer, C.A., Puig, P., Orange, D.L., 2004. Sediment deposition in a modem submarine canyon: Eel Canyon, northern California. Marine Geology 211, 101-119.
Neill, S.P., Scourse, J.D., 2009. The formation of headland/island sandbanks. Continental Shelf Research 29, 2167-2177.
Nickols, K.J., Gaylord, B., Largier, J.L., 2012. The coastal boundary layer: predictable current structure decreases alongshore transport and alters scales of dispersal. Marine Ecology Progress Series 464, 17-35.
Patsch, K., Griggs, G., 2007. Development of Sand Budgets for California's Major Littoral Cells. Institute of Marine Sciences, University of California, Santa Cruz, p. 115.
Pattiaratchi, C., James, A., Collins, M., 1987. Island wakes and headland eddies: A comparison between remotely sensed data and laboratory experiments. Journal of Geophysical Research: Oceans 92, 783-794.
Perg, L.A., Anderson, R.S., Finkel, R.C., 2003. Use of cosmogenic radionuclides as a sediment tracer in the Santa Cruz littoral cell, California, United States. Geology 31, 299-302.
Ris, R.C., Holthuijsen, L.H., Booij, N., 1999. A third-generation wave model for coastal regions - 2. Verification. Journal of Geophysical Research-Oceans 104, 7667-7681.
Roughan, M., Mace, A.J., Largier, J.L., Morgan, S.G., Fisher, J.L., Carter, M.L., 2005. Subsurface recirculation and larval retention in the lee of a small headland: A variation on the upwelling shadow theme. Journal of Geophysical Research-Oceans 110.
Sallenger, A.H., Krabill, W., Brock, J., Swift, R., Manizade, S., Stockdon, H., 2002. Sea-cliff erosion as a function of beach changes and extreme wave runup during the 1997-1998 El Nino. Marine Geology 187, 279-297.
Sanderson, P.G., Eliot, I., 1999. Compartmentalisation of beachface sediments along the southwestern coast of Australia. Marine Geology 162, 145-164.

Scholar, D.C., Griggs, G.B., 1997. Pocket Beaches of California: Sediment Transport Along a Rocky Coastline, Proceedings of California's Coastal Natural Hazards. University of Southern California Sea Grant Program, Santa Barbara, pp. 65-75.
Scott, T., Masselink, G., Russell, P., 2011. Morphodynamic characteristics and classification of beaches in England and Wales. Marine Geology 286, 1-20.
Short, A.D., 1999. Handbook of beach and shoreface morphodynamics. John Wiley, New York.
Signell, R.P., Geyer, W.R., 1991. Transient Eddy Formation around Headlands. Journal of Geophysical Research-Oceans 96, 2561-2575.
Silva, R., Baquerizo, A., Losada, M.A., Mendoza, E., 2010. Hydrodynamics of a headland-bay beach-Nearshore current circulation. Coastal Engineering 57, 160-175.
Slagel, M.J., Griggs, G.B., 2008. Cumulative losses of sand to the California coast by dam impoundment. Journal of Coastal Research 24.
Soulsby, R., 1997. Dynamics of Marine Sands: A Manual for Practical Applications. Thomas Telford, London.
Storlazzi, C.D., Field, M.E., 2000. Sediment distribution and transport along a rocky, embayed coast: Monterey Peninsula and Carmel Bay, California. Marine Geology 170, 289-316.
Storlazzi, C.D., Reid, J.A., 2010. The influence of El Nino-Southern Oscillation (ENSO) cycles on wave-driven sea-floor sediment mobility along the central California continental margin. Continental Shelf Research 30, 1582-1599.
Stuiver, C., 2013. Coastal evolution of soft cliff coasts: headland formation and evolution on the Southwest Isle of Wight, Engineering and the Environment. University of Southampton, p. 277.
Stul, T., Gozzard, J., Eliot, I., Eliot, M., 2012. Coastal Sediment Cells between Cape Naturaliste and the Moore River, Western Australia in: Transport, W.A.D.o. (Ed.). Damara WA Pty Ltd and Geological Survey of Western Australia, Fremantle, WA, Australia, p. 44.
van Rijn, L.C., 2010. Coastal erosion control based on the concept of sediment cells. CONSCIENCE, Deltares, The Netherlands, p. 80.
Winant, C.D., 2006. Three-dimensional wind-driven coastal circulation past a headland. Journal of Physical Oceanography 36, 1430-1438.
Wingfield, D.K., Storlazzi, C.D., 2007. Spatial and temporal variability in oceanographic and meteorologic forcing along Central California and its implications on nearshore processes. Journal of Marine Systems 68.
Wright, L., Short, A., 1984. Morphodynamic Variability of Surf Zones and Beaches - A Synthesis. Marine Geology 56, 93-118.
Young, A.P., Ashford, S.A., 2006. Application of airborne LIDAR for seacliff volumetric change and beach-sediment budget contributions. Journal of Coastal Research 22, 307-318.

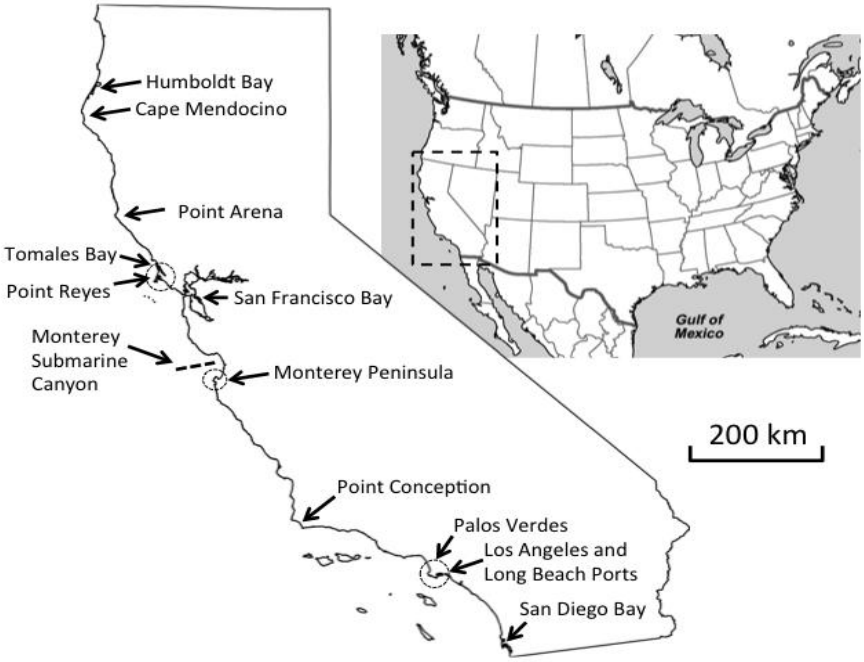

Fig. 1

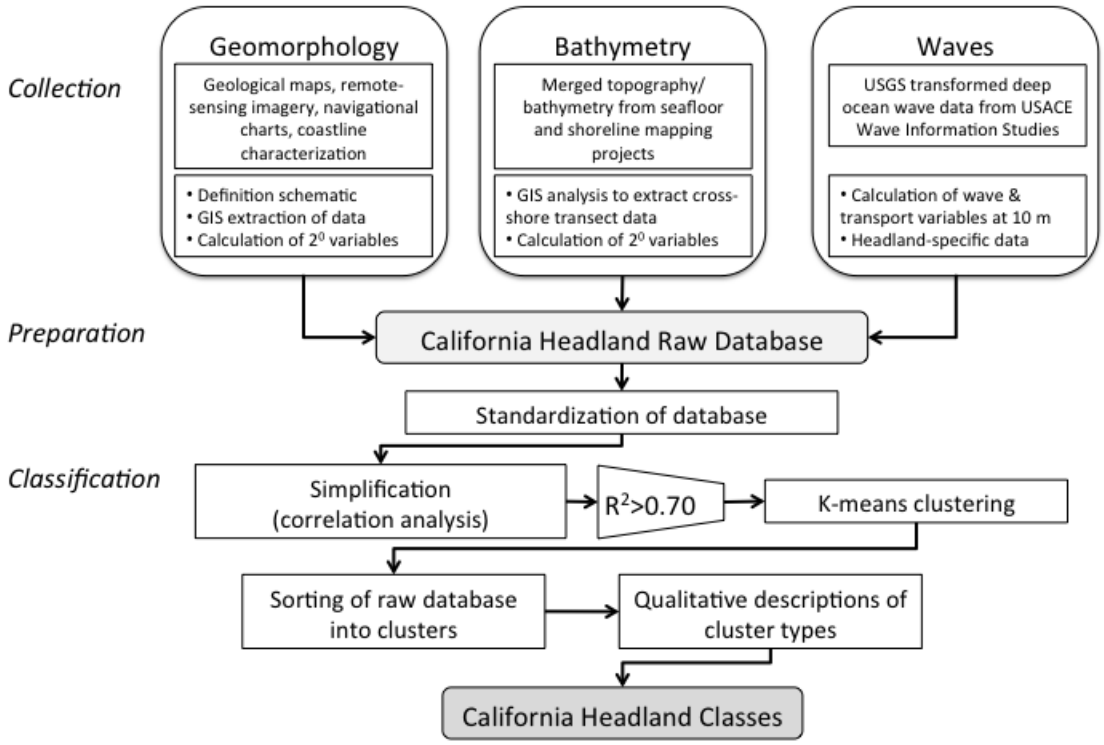

Fig. 2

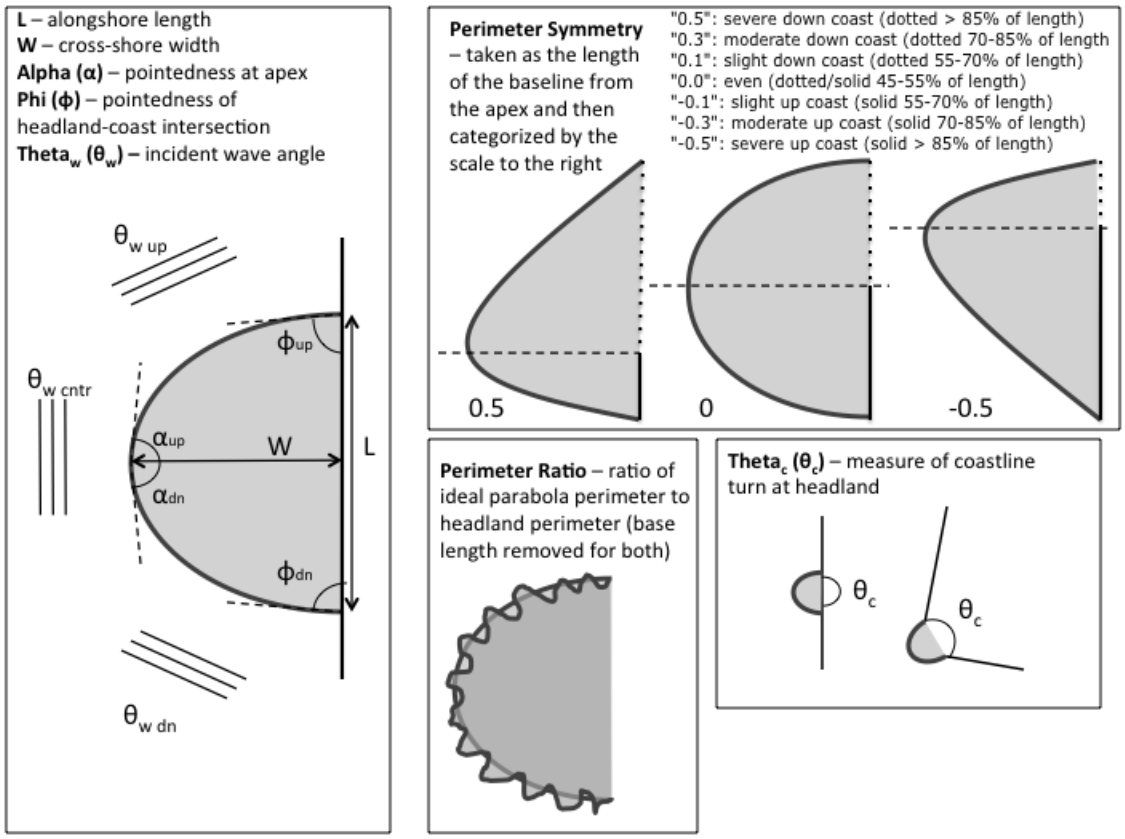

Fig. 3

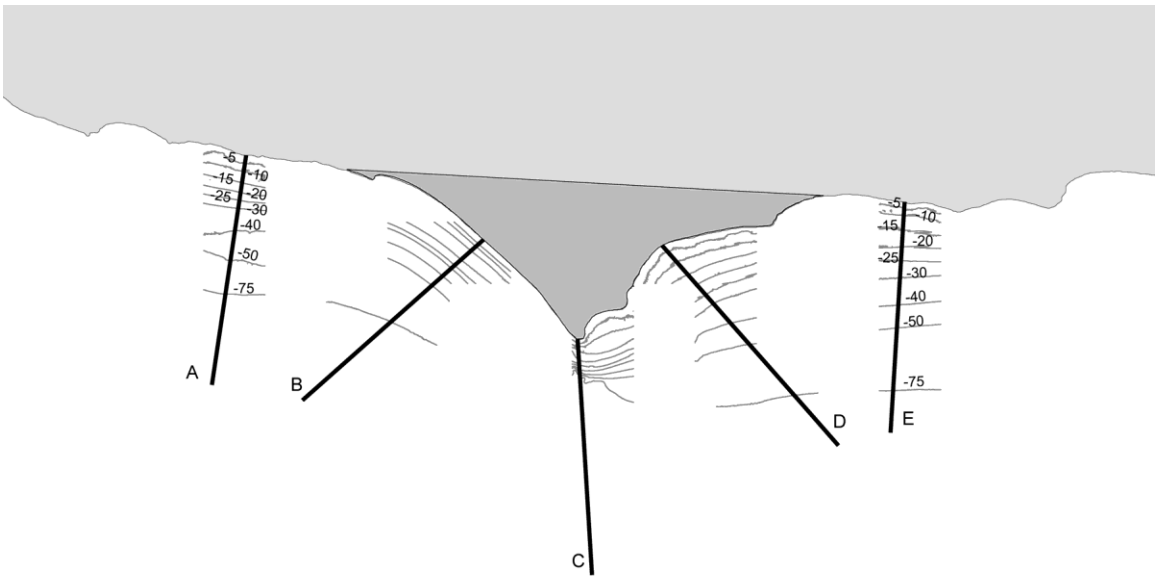

Fig. 4

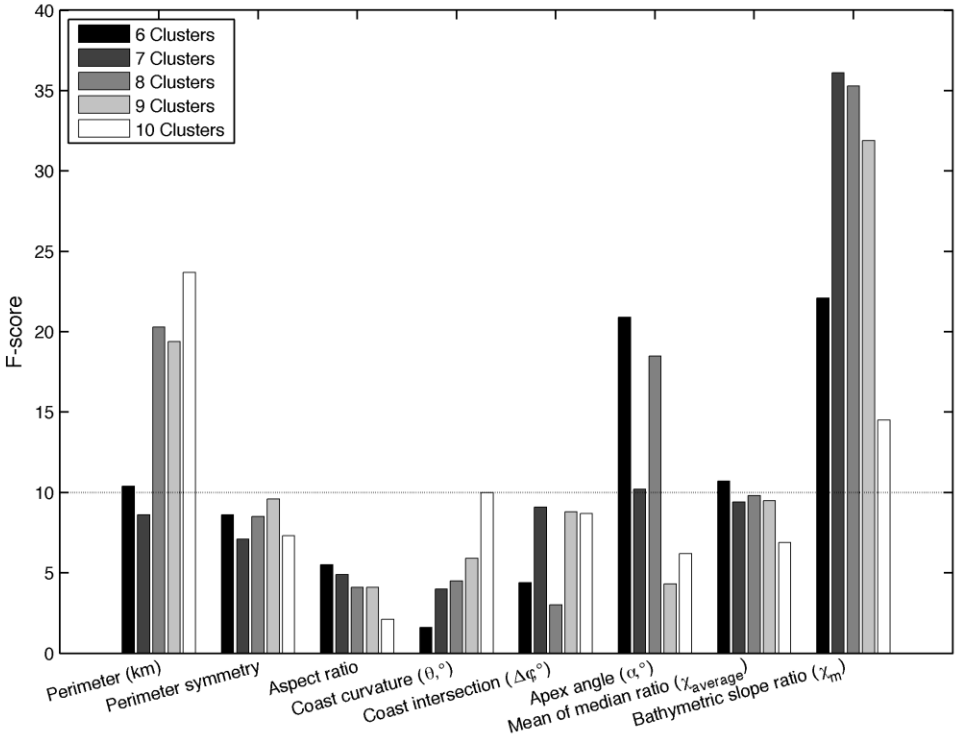

Fig. 5

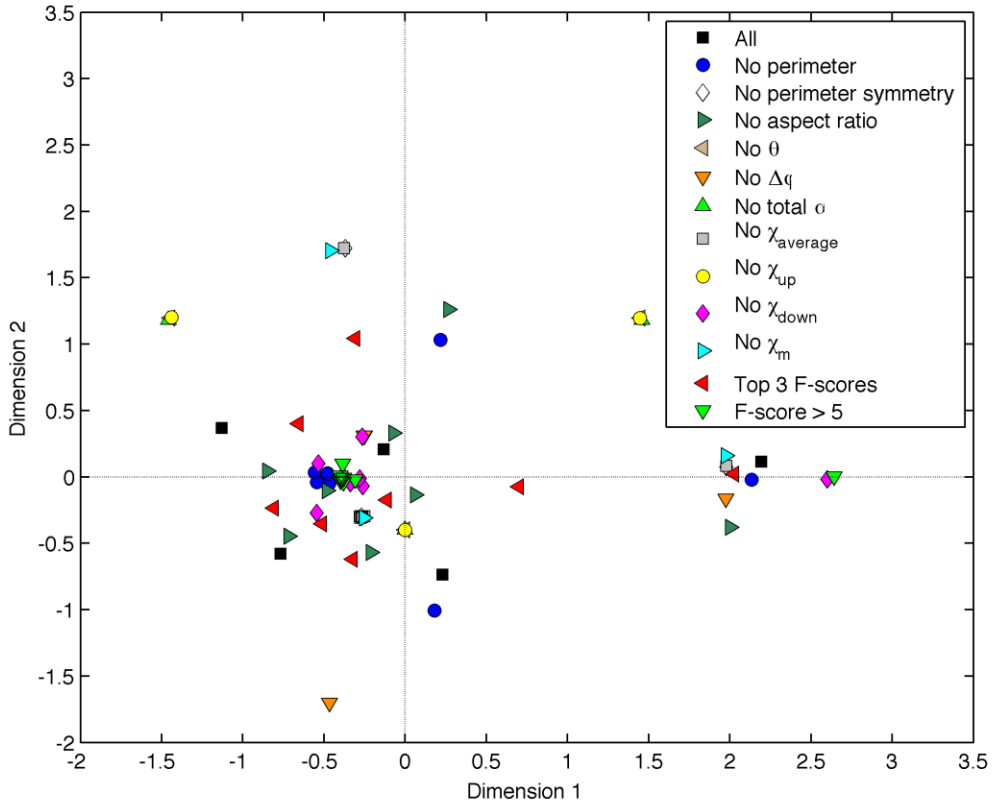

Fig. 6

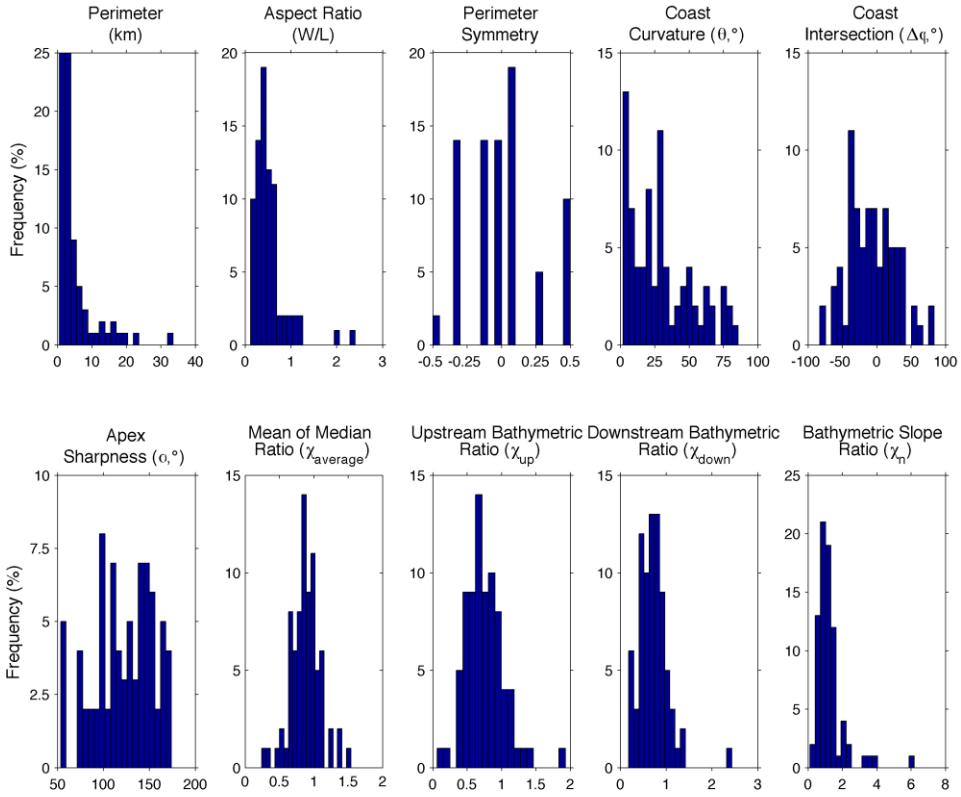

Fig. 7

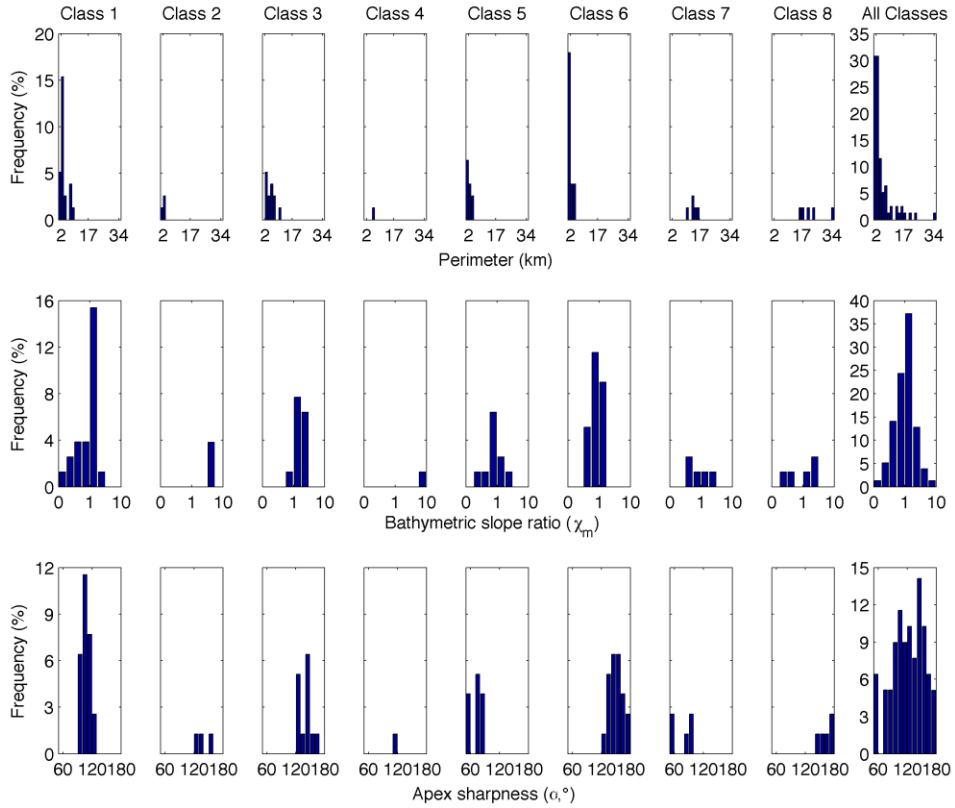

Fig. 8

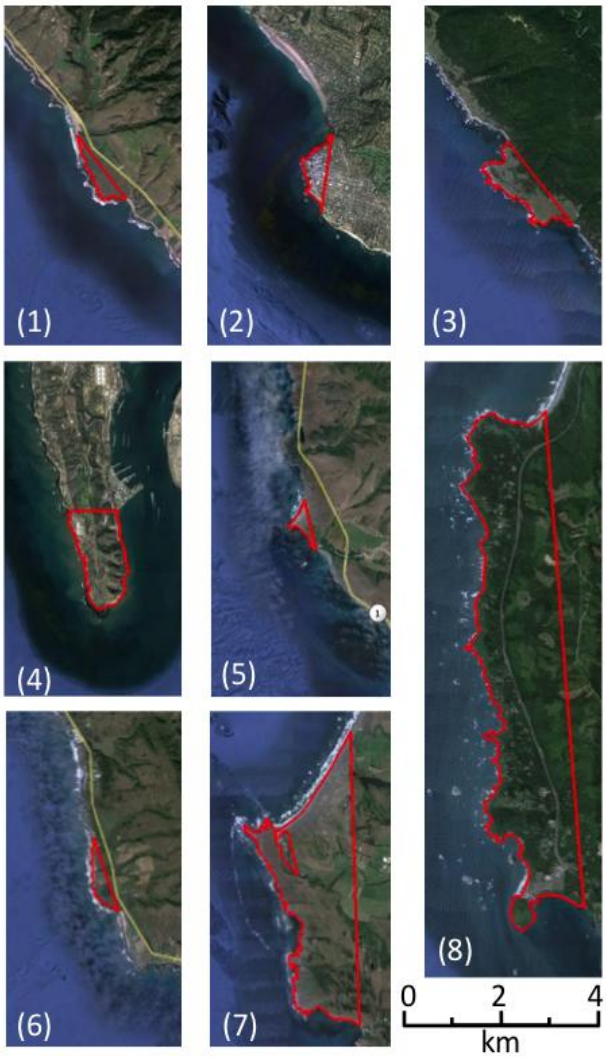

Fig. 9

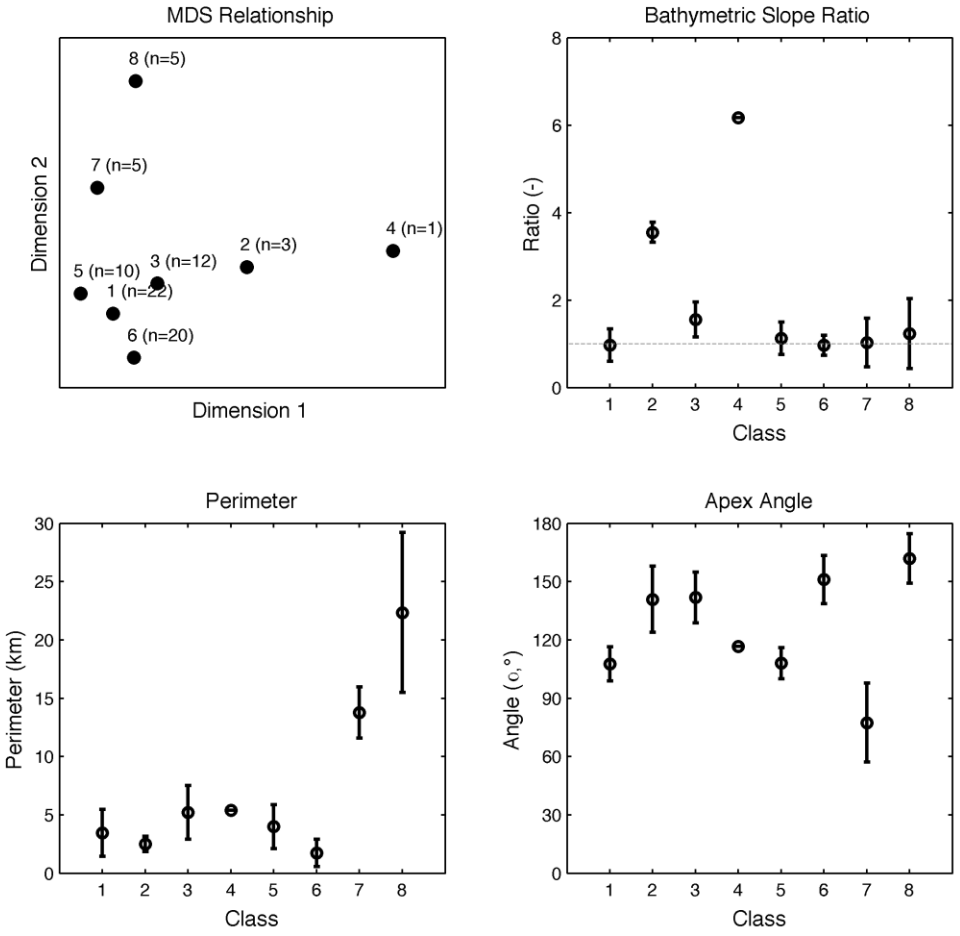

Fig. 10

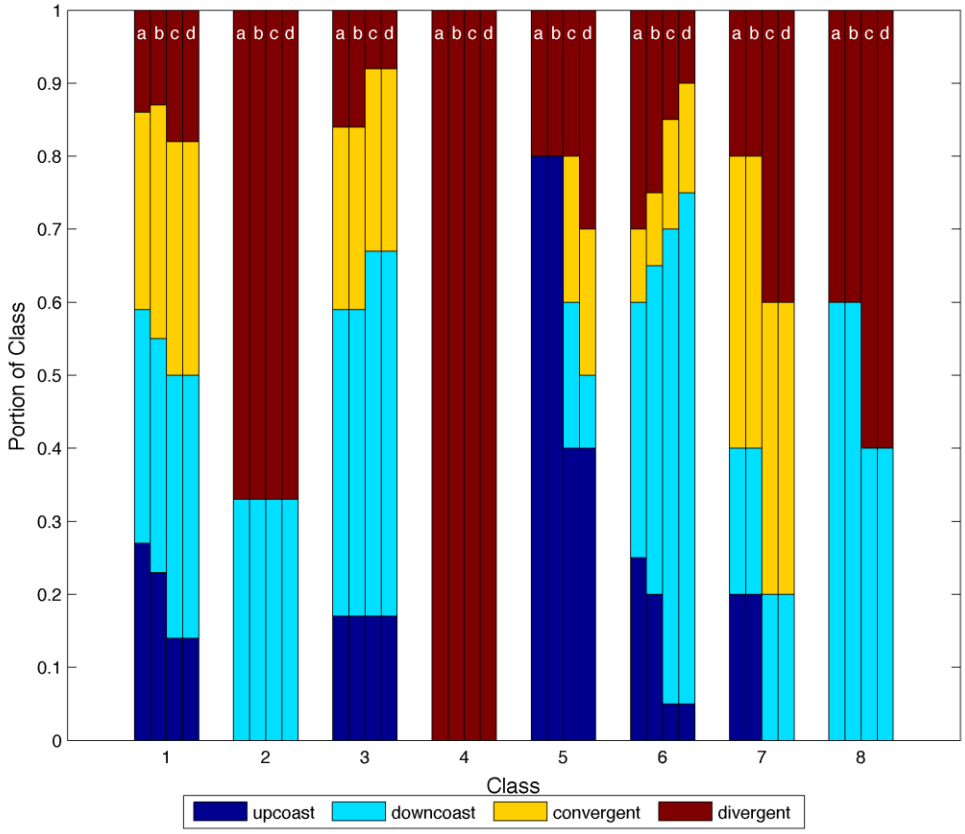

Fig. 11

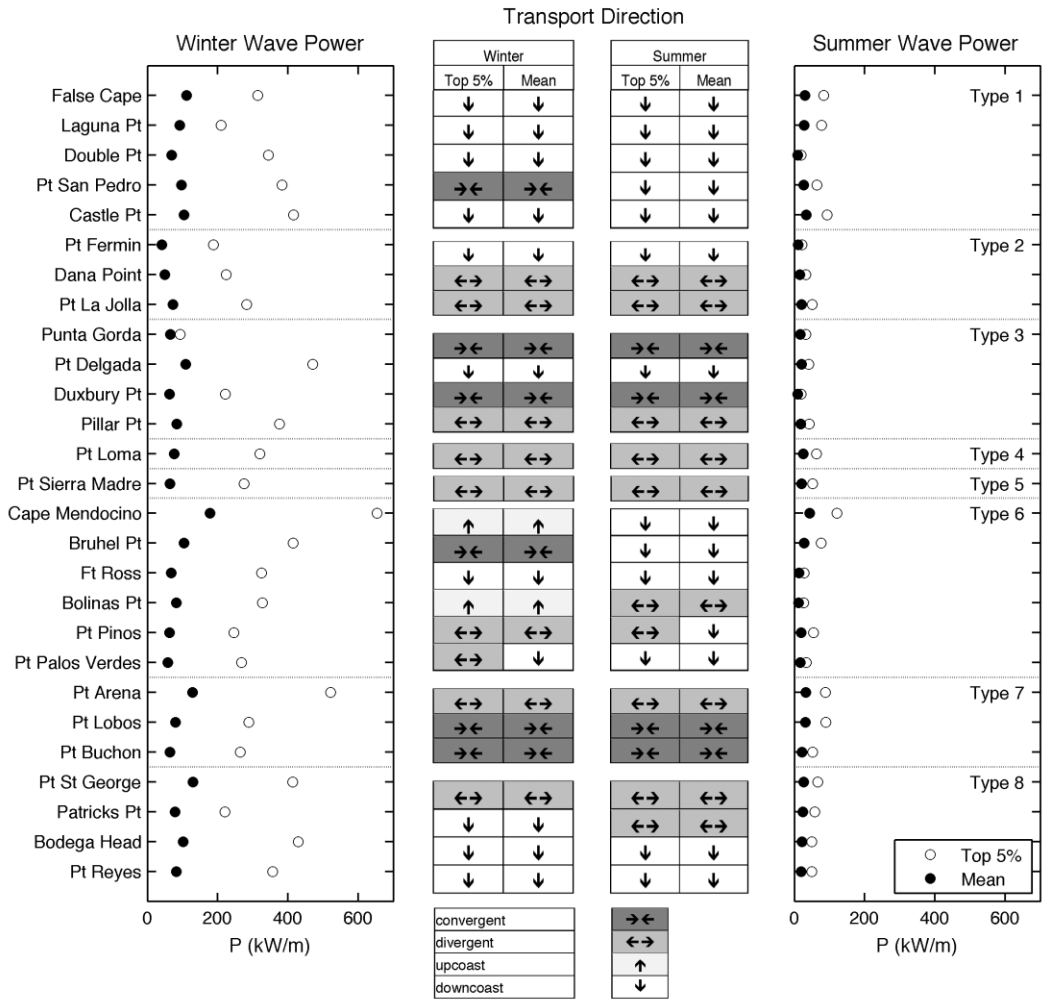

Fig. 12

Highlights

- Eight headland classes were built from geomorphic and bathymetric parameters.
- The classifying parameters are perimeter, bathymetric slope ratio, and apex angle.
- Three types of headlands appear to function well as littoral cell boundaries.
- The headland classes cast doubt on traditional California littoral cell boundaries.